NAVY DEPARTMENT

DAVID TAYLOR MODEL BASIN

[redacted]

HYDROMECHANICS

○

AERODYNAMICS

○

STRUCTURAL MECHANICS

○

APPLIED MATHEMATICS

A PROCEDURE FOR COMPUTING STRESSES IN A CONICAL SHELL NEAR RING STIFFENERS OR REINFORCED INTERSECTIONS

by

Richard V. Raetz and John G. Pulos

STRUCTURAL MECHANICS LABORATORY

RESEARCH AND DEVELOPMENT REPORT

April 1958

Report 1015

A PROCEDURE FOR COMPUTING STRESSES IN A CONICAL SHELL NEAR RING STIFFENERS OR REINFORCED INTERSECTIONS

by

Richard V. Raetz and John G. Pulos

April 1958

Report 1015
NS 731-038

TABLE OF CONTENTS

	Page
ABSTRACT	1
INTRODUCTION	1
GENERAL CONSIDERATIONS	2
COMPUTATION OF STRESSES AND STRAINS	3
DETERMINATION OF EDGE FORCES H_i AND MOMENTS M_i	7
CASE A: UNSTIFFENED INTERSECTION OF CONICAL AND CYLINDRICAL SHELLS OF DIFFERENT THICKNESSES, SUBJECT TO EXTERNAL HYDROSTATIC PRESSURE	8
CASE B: CONICAL OR CYLINDRICAL SHELLS WITH CLAMPED EDGES, SUBJECT TO EXTERNAL HYDROSTATIC PRESSURE	11
CASE C: INTERSECTION OF CONICAL AND CYLINDRICAL SHELLS REINFORCED BY A STIFFENER OF FINITE RIGIDITY, SUBJECT TO EXTERNAL HYDROSTATIC PRESSURE	12
CASE D: EFFECT OF A HEAVY FORGED-RING TYPE STIFFENER UPON THE INTERSECTION DEFORMATIONS	13
APPLICABILITY OF METHOD	16
ACKNOWLEDGMENTS	18
APPENDIX A - NUMERICAL EXAMPLE	19
APPENDIX B - GECKELER APPROXIMATION FOR CONICAL SHELLS	25
APPENDIX C - DERIVATION OF THE STRESS AND STRAIN EXPRESSIONS, EQUATIONS [1] THROUGH [5]	27
REFERENCES	32

LIST OF ILLUSTRATIONS

Page

Figure 1 - Notation for Conical Shell Element 3

Figure 2 - Graph of ζ, θ, ψ, and ϕ Functions 6

Figure 3 - Graph of F_a, F_b, F_c, and F_d Functions 6

Figure 4 - Notation for Cone-Cylinder Juncture 8

Figure 5 - Reinforced Cone-Cone Juncture 12

Figure 6 - Notation for Reinforcement at Cone-Cylinder Juncture 14

Figure 7 - Schematic Drawing of Illustrative Model 19

Figure 8 - Theoretical and Experimental Circumferential Strains in Illustrative Model for External Hydrostatic Pressure of 1 PSI 23

Figure 9 - Theoretical and Experimental Longitudinal Strains on External and Internal Surfaces of Illustrative Model for External Hydrostatic Pressure of 1 PSI 24

LIST OF TABLES

TABLE 1 - Functions Defining Bending Action of Shell 7

TABLE 2 - Calculation Sheet for Computing Stresses and Strains at Large-Diameter End of Cone in Illustrative Example 21

NOTATION

a, b, c, d, f, g	Coefficients representing edge rotation and displacement per unit edge or surface load
E	Young's Modulus
h_i	Shell thickness
H_i	Discontinuity shearing force normal to axis of symmetry
M_i	Discontinuity bending moment in a meridional plane
p	Hydrostatic pressure
Q_i	Discontinuity shearing force normal to shell surface
R	Radial distance from axis of symmetry
U	$\sqrt[4]{12\,(1-\nu^2)}$
$\overline{w}$	Displacement perpendicular to axis of shell
x	Coordinate taken along shell generator, measured from juncture or base of cone
y	Coordinate taken along cone generator, measured from apex of cone
α_i	Angle between axis of cone and generator
β_i	$\sqrt[4]{\dfrac{3\,(1-\nu^2)\cos^2\alpha_i}{R_i^2 h_i^2}}$
ϵ	Strain
ν	Poisson's ratio
σ	Stress
$\phi, \zeta, \psi, \theta, F_a, F_b, F_c, F_d$	Functions defining bending action of the shell
θ	Axial rotation of shell
D	$\dfrac{E h^3}{12\,(1-\nu^2)}$, flexural rigidity of shell
δ_1, δ_2	Ring dimensions associated with Figure 6

ABSTRACT

A second approximation to the complete theory for the axisymmetric deformations of thin elastic conical shells, as derived by E. Meissner and F. Dubois, is presented. This simplification of the exact differential equation leads to a so-called Geckeler-type approximation for conical shells.

From this approximation, a step-by-step numerical procedure is developed for calculating stresses and strains throughout the conical elements of shell structures. The methods include computation of the edge shearing forces and bending moments which arise from discontinuity effects at cone-cone and cone-cylinder junctures, either with or without transverse reinforcing rings.

The range of applicability of the approximation is also discussed.

INTRODUCTION

Because of the increasingly frequent use of conical shells in the pressure hulls of submarines, a simplified procedure has been developed by which the elastic behavior of these structural elements may be easily computed. The method makes use of exponential and trigonometric functions for determining the axisymmetric discontinuity stresses and strains at either end of a truncated cone joined to another cone or to a cylinder with or without transverse reinforcement at the intersection, or those at or near stiffeners on semi-infinite cones. The analysis underlying this computational procedure follows closely the Geckler approximation[1] to the more rigorous Love-Meissner equations of equilibrium for shells of revolution.[2]

The use of a Geckeler-type approximation for analyzing stresses in conical shells has long been employed in the pressure-vessel industry. However, when design calculations for steep conical transition sections on submarines were first required in 1951, it was not known whether the approximation was sufficiently accurate for the strength analysis of submarine pressure hulls. A study of the exact Love-Meissner theory, as applied to conical shells by Dubois[3] and Watts and Burrows[4] showed it to be impracticable for reinforced cone-cylinder intersections. There was then developed by Wenk and Taylor[5] a first approximation to the complete theory which would facilitate analysis of reinforced junctures. These same authors later presented a different form[6] of the exact solution and one from which the errors involved in an approximate solution could be specifically evaluated. Their results included a statement of edge coefficients for conical shells which provided a convenient method for analyzing the reinforced intersections at both the large and small ends of truncated cones. The results published in TMB Reports 826[5] and 981[6] were evaluated experimentally and were found valid.[7]

---

[1]References are listed on page 32.

In a search for more rapid methods of computation, a second approximation to the complete theory which is essentially the Geckeler-type approximation for conical shells was reconsidered. For the geometries of interest to submarine designers this further approximation was found to differ but little from the more rigorous analyses.[5,6] Also, as might be expected, this Geckeler-type approximation was more reducible to a step-by-step form of computation. The numerical procedure resulting from this simplified analysis is presented in this report. First, equations for computing stresses and strains throughout a conical shell as a function of edge forces and moments and the hydrostatic pressure loading are presented. Next, equations are provided for computing these edge forces and moments where the cone element is joined to another cone or cylinder, with or without transverse reinforcement at the common juncture. A numerical example is then given in Appendix A showing in tabular form the routine by which stresses and strains may be computed for a structure composed of two cylindrical shells of different diameters joined by a conical transition section and having reinforcing rings at both intersections.

The derivation of this second approximation to the complete theory for conical shells and its justification are presented in Appendix B. The formulas for stresses and strains resulting from this analysis are derived in Appendix C.

GENERAL CONSIDERATIONS

In accordance with general methods for evaluating discontinuity stresses at shell intersections, an unstiffened truncated section of cone, which is assumed to have a length sufficient that the boundary conditions at one end do not disturb membrane deformations at the other, is isolated for study. Under pressure loading, the stresses and displacements everywhere in the shell are the sum of the membrane terms and additional terms corresponding to discontinuity shear and moment loads uniformly distributed on the periphery of each boundary. These discontinuity effects, considered to be axisymmetrical, depend on the contiguous structure to which the conical element is joined. They result from the fact that the membrane deformations which would occur in each member, separately, under pressure loading are not identical so that the edges of the several elements theoretically would deform different amounts and hence would not match. To enforce compatibility of displacements and rotations of the intersecting elements such a discontinuity can be eliminated by the introduction of additional forces and moments at the edges of each component shell. These, of course, must themselves satisfy equilibrium conditions. The method is readily applied to cone-cylinder and cone-cone junctures.

If transverse reinforcement in the form of a ring stiffener is provided at the intersection, a corresponding analysis is made with the additional feature that compatibility of displacements and rotations is required of both the shell components and the stiffener at the common juncture. As another special case, stresses near ring stiffeners in a reinforced conical shell are obtained simply by considering the large end of one semi-infinite cone joined to the small

end of another semi-infinite cone of equal apex angle, with a transverse ring at their intersection. In considering the reinforced-intersection problem, it is first assumed that the stiffening rings are very narrow and thin so that there is practically line contact around the circumference at the common juncture of the three elements—the ring and the two axisymmetric shells—and that the ring properties are concentrated on this line. However, if the intersection is reinforced by a heavy forged-ring type of stiffener with appreciable cross-sectional dimensions, then the assumption of line concentration is no longer valid, and the analysis is extended to include the effects of such finite width and depth upon the intersection deformations.

Particular cases of composite structures such as these are discussed in further detail, and final formulas for the discontinuity shears and moments are given in this report. The analysis of composite structures including other components, such as spherical, elliptical, and toroidal shells of revolution follows closely that described in this report, and suggestions are given for extending the present results to such cases.

COMPUTATION OF STRESSES AND STRAINS

A thin-walled shell, such as a cone or a cylinder, develops only membrane stresses and strains when loaded solely by uniform hydrostatic pressure provided that the edges of the shell are unrestrained. However, in reality the edges of such shell structures must be restrained in some manner, i.e., attachment to other components or foundations or closures to make them pressure-tight. In the vicinity of these restrained edges, local bending stresses are developed in addition to the uniform membrane stresses. Formulas are presented herein for determining the total stresses and strains which arise from the superposition of these discontinuity and membrane effects.

The nomenclature and sign conventions used in the analysis of a truncated conical shell are defined in Figure 1. These are applicable whether the edge of the shell under consideration is the large- or small-diameter end of the cone, or the end of a cylinder, which is taken to be the limiting case of a truncated cone (either end) as the angle α_i approaches zero. Note that x is the distance along the generator of the shell measured from the edge under consideration and not the distance from the cone apex as in Reference 5.

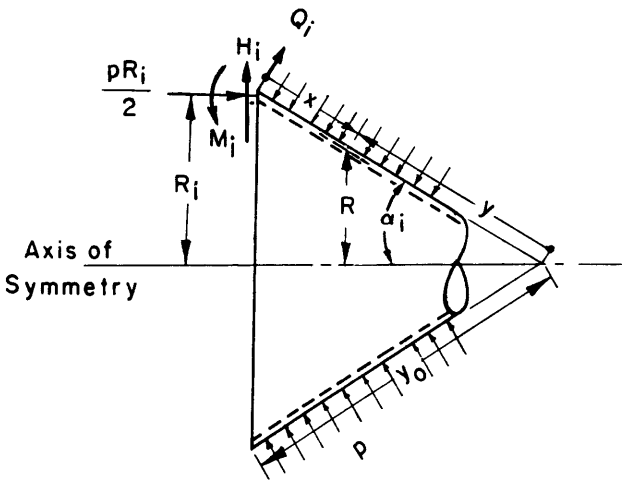

Figure 1 - Notation for Conical Shell Element

A bending moment M_i is considered positive if it tends to put the outer surface of the

shell in tension, and a shearing force H_i is considered positive when it acts in a direction away from the axis of symmetry. The transverse shearing force Q_i is composed of the radial shear component H_i and the axial force $pR_i/2$. A hydrostatic pressure p is considered positive when it is external; for internal pressure p is negative. The subscript i is used to distinguish the structural elements from each other where an intersection composed of two or more such elements is being analyzed.

The quantities H_i and M_i are discontinuity shears and moments arising from the intersections of various shell elements with each other and with stiffening rings. They may be determined in terms of the shell geometry and elasticity and the surface loading by enforcing conditions of force and moment equilibrium and continuity of radial displacement and axial rotation at the juncture.

Once the discontinuity shears H_i (or Q_i) and moments M_i are known, the following formulas may be used for determining the longitudinal and circumferential stresses and strains in each shell element as functions of the distance x from the shell edge under study:
Longitudinal stresses (the upper sign is for the external fiber and the lower sign for the internal fiber):

$$\sigma_x = -\frac{pR}{2h_i \cos\alpha_i} + 2\frac{\beta_i}{h_i} M_i \tan\alpha_i \left[\frac{Q_i}{2\beta_i M_i}\psi + \zeta\right] \pm \frac{6M_i}{h_i^2}\left[\phi - \frac{Q_i}{\beta_i M_i}\zeta\right] \qquad [1]$$

Circumferential stresses:

$$\sigma_\phi = -\frac{pR}{h_i \cos\alpha_i}\left(1 - \frac{\nu}{2}\right) - \frac{U^2 M_i}{h_i^2}\left(\psi - \frac{Q_i}{\beta_i M_i}\theta\right) + \nu\sigma_x \qquad [2]$$

Longitudinal strain (external fiber):

$$\epsilon_x = -\frac{pR}{2Eh_i \cos\alpha_i}(1 - 2\nu) + 2\frac{\beta_i}{Eh_i}(1 - \nu^2) M_i \tan\alpha_i \left[\frac{Q_i}{2\beta_i M_i}\psi + \zeta\right] + \frac{M_i}{Eh_i^2}\left[F_a - \frac{Q_i}{\beta_i M_i} F_b\right] \qquad [3]$$

Longitudinal strain (internal fiber):

$$\epsilon_x = -\frac{pR}{2Eh_i \cos\alpha_i}(1-2\nu) + 2\frac{\beta_i}{Eh_i}(1-\nu^2)M_i \tan\alpha_i \left[\frac{Q_i}{2\beta_i M_i}\psi + \zeta\right] + \frac{M_i}{Eh_i^2}\left[F_c - \frac{Q_i}{\beta_i M_i}F_d\right] \quad [4]$$

Circumferential strain (all fibers throughout shell thickness):

$$\epsilon_\phi = -\frac{pR}{Eh_i \cos\alpha_i}\left(1-\frac{\nu}{2}\right) - \frac{U^2 M_i}{Eh_i^2}\left[\psi - \frac{Q_i}{\beta_i M_i}\theta\right] \quad [5]$$

In these expressions

$$\beta_i = \sqrt[4]{\frac{3\cos^2\alpha_i}{R_i^2 h_i^2}(1-\nu^2)} = 1.2854\sqrt{\frac{\cos\alpha_i}{R_i h_i}}; \text{ for } \nu = 0.3 \quad [6]$$

and

$$U = \sqrt[4]{12(1-\nu^2)} = 1.81784; \text{ for } \nu = 0.3$$

Equations [1] through [5] are derived in Appendix C.

It should be noted that for a conical shell the radius R varies linearly with the coordinate distance x, i.e., $R = R_i \pm x \sin\alpha_i$ where the minus sign applies to the large end and the plus sign to the small end of a truncated cone. In the limiting case as the half apex angle $\alpha_i \to 0$, Formulas [1] through [5] reduce to analogous expressions for a circular cylindrical shell for which case the radius R now becomes a constant.

The functions ϕ, ζ, ψ, θ, F_a, F_b, F_c, and F_d used in computing the bending terms in Equations [1] through [5] are defined by the following:

$$\phi(\beta x) = e^{-\beta x}(\cos\beta x + \sin\beta x); \quad \theta(\beta x) = e^{-\beta x}\cos\beta x$$

$$\psi(\beta x) = e^{-\beta x}(\cos\beta x - \sin\beta x); \quad \zeta(\beta x) = e^{-\beta x}\sin\beta x \quad [7]$$

$$F_{a,c}(\beta x) = \pm 6(1-\nu^2)\phi(\beta x) + \nu\sqrt{12(1-\nu^2)}\,\psi(\beta x)$$

$$F_{b,d}(\beta x) = \pm 6(1-\nu^2)\zeta(\beta x) + \nu\sqrt{12(1-\nu^2)}\,\theta(\beta x)$$

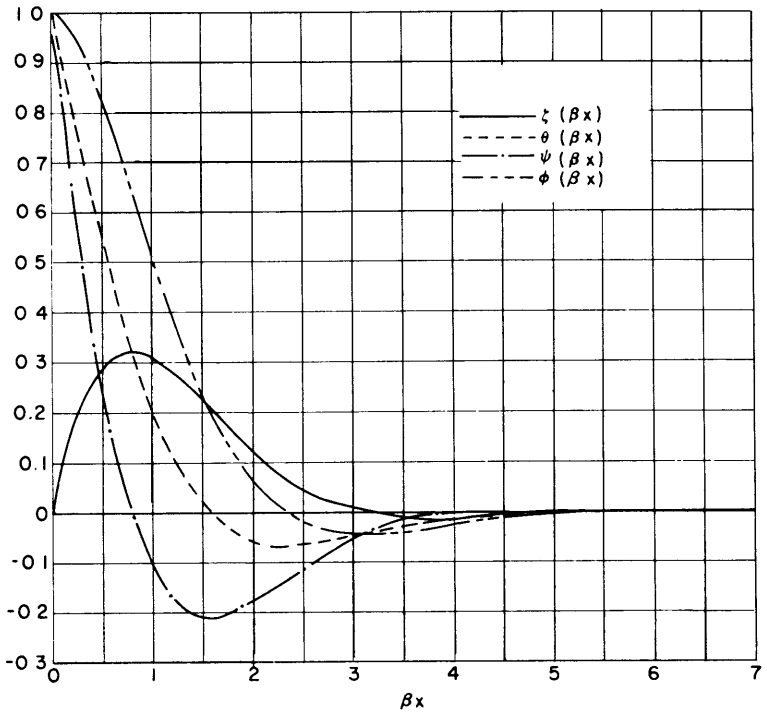

Figure 2 - Graph of ζ, θ, ψ, and ϕ Functions

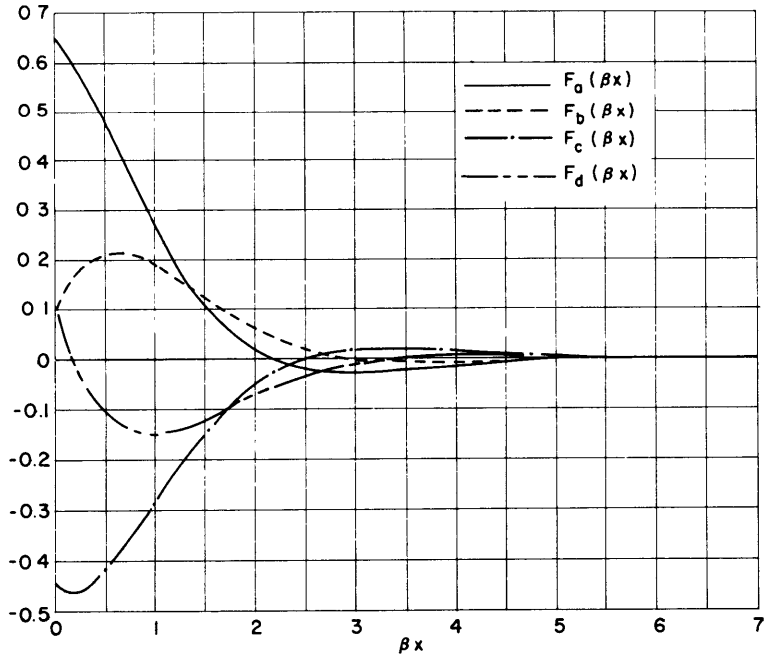

Figure 3 - Graph of F_a, F_b, F_c, and F_d Functions

where the plus signs apply to F_a and F_b and the minus signs to F_c and F_d; they are all functions of the dimensionless variable βx. These quantities computed for several values of βx are given in Table 1 and represented graphically in Figures 2 and 3. It is seen that all the functions approach zero as the quantity βx becomes large. This indicates that the bending produced in the shells by the discontinuity forces and moments is actually local and damps out rapidly away from the loaded edge. In practice, it is convenient to choose values of βx which appear in Table 1 so that interpolation will not be necessary. From these and with β computed from Equation [6] the corresponding values of x can easily be found, and the stress and strain distributions may then be determined using Equations [1] through [5]. The procedure for carrying out these computations is illustrated in Appendix A.

TABLE 1

Functions Defining Bending Action of Shell

βx	ϕ	ψ	Θ	ζ	F_a	F_b	F_c	F_d
0	1.0000	1.0000	1.0000	0	6.4514	0.9914	-4.4686	0.9914
0.1	0.9907	0.8100	0.0903	0.0903	6.2122	1.3855	-4.6062	0.3995
0.2	0.9651	0.6398	0.8024	0.1627	5.9037	1.6838	-4.6351	-0.0928
0.3	0.9267	0.4888	0.7077	0.2189	5.5444	1.8968	-4.5752	-0.4936
0.4	0.8784	0.3564	0.6174	0.2610	5.1494	2.0372	-4.4428	-0.8130
0.6	0.7628	0.1431	0.4530	0.3099	4.3068	2.1412	-4.0230	-1.2430
0.8	0.6354	-0.0093	0.3131	0.3223	3.4601	2.0702	-3.4785	-1.4494
1.0	0.5083	-0.1108	0.1988	0.3096	2.6655	1.8875	-2.8851	-1.4933
1.2	0.3899	-0.1716	0.1091	0.2807	1.9588	1.6408	-2.2990	-1.4244
1.4	0.2849	-0.2011	0.0419	0.2430	1.3562	1.3683	-1.7550	-1.2853
1.6	0.1959	-0.2077	-0.0059	0.2018	0.8637	1.0960	-1.2755	-1.1076
1.7	0.1576	-0.2047	-0.0235	0.1812	0.6576	0.9661	-1.0634	-1.0127
1.8	0.1234	-0.1985	-0.0376	0.1610	0.4770	0.8418	-0.8706	-0.9164
1.85	0.1078	-0.1945	-0.0433	0.1511	0.3958	0.7821	-0.7814	-0.8679
1.9	0.0932	-0.1899	-0.0484	0.1415	0.3206	0.7246	-0.6972	-0.8206
2.0	0.0667	-0.1794	-0.0563	0.1230	0.1864	0.6158	-0.5420	-0.7274
2.2	0.0244	-0.1548	-0.0652	0.0895	-0.0203	0.4241	-0.2867	-0.5533
2.6	-0.0254	-0.1019	-0.0636	0.0383	-0.2397	0.1461	0.0377	-0.2721
3.0	-0.0423	-0.0563	-0.0493	0.0071	-0.2868	-0.0101	0.1752	-0.0877
3.4	-0.0408	-0.0237	-0.0323	-0.0085	-0.2463	-0.0784	0.1993	0.0144
4.0	-0.0258	0.0019	-0.0120	-0.0139	-0.1390	-0.0878	0.1428	0.0640
5.0	-0.0046	0.0084	0.0019	-0.0065	-0.0168	-0.0336	0.0334	0.0374
7.0	0.0013	0.0001	0.0007	0.0006	0.0072	0.0040	-0.0070	-0.0026

DETERMINATION OF EDGE FORCES H_i AND MOMENTS M_i

The discontinuity forces and moments which arise from a mismatch of membrane deformations in intersecting shells may be determined from considerations of force and moment equilibrium and of compatibility of rotations and displacements of the edges of the component shells at the common juncture. The unit edge rotations and displacements can be expressed in terms of edge coefficients such as those defined and discussed in References 5 and 6.

These edge coefficients are functions of the geometry and elasticity of the two intersecting component shells; they represent the amount of axial rotation and radial displacement per unit edge bending moment, unit edge shearing force, and unit surface pressure. The total rotation θ_i and displacement $\bar{w}_i$ of the edge for combined loading are then obtained by superposition, i.e.,

$$\theta_i = a_i M_i + b_i H_i + c_i p$$
$$\bar{w}_i = d_i M_i + g_i H_i + f_i p \qquad [8]$$

where a_i, b_i, c_i, d_i, f_i, and g_i are defined as the edge coefficients.

The method of using edge coefficients is general and is very convenient in the analysis of any composite structure, such as those encountered in pressure-vessel design. Here we shall consider in detail the intersections of conical and cylindrical shells, a typical case of which is shown schematically in Figure 4 with the discontinuity forces and moments acting at the shell edges, and treat particular cases of interest in the field of submarine pressure-hull design.

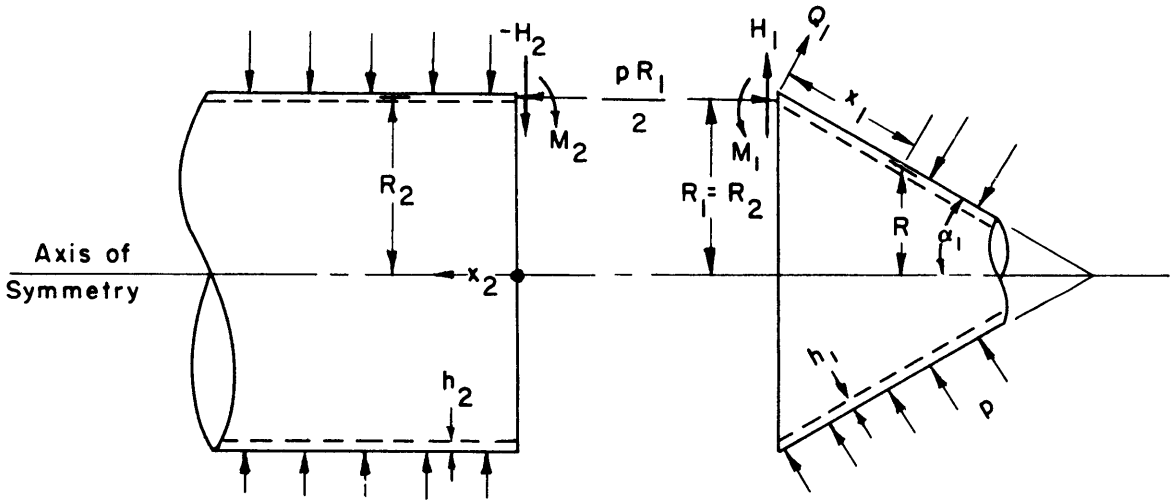

Figure 4 - Notation for Cone-Cylinder Juncture

CASE A: UNSTIFFENED INTERSECTION OF CONICAL AND CYLINDRICAL SHELLS OF DIFFERENT THICKNESSES, SUBJECT TO EXTERNAL HYDROSTATIC PRESSURE

In this analysis of the intersection of two shells of revolution, it should be recalled that each component shell is assumed to be sufficiently long that the boundary conditions at the far ends do not affect those at the common juncture.

When two such shells, identified by $i = 1$ and $i = 2$, are joined together with no transverse reinforcement at their intersection, the discontinuity bending moment and radial shearing

force may be determined from the following expressions:

$$M_1 = \left[\frac{\bar{f}\bar{b} - \bar{c}\bar{g}}{\bar{a}\bar{g} - \bar{b}\bar{d}}\right] p = M_2$$

$$H_1 = \left[\frac{\bar{c}\bar{d} - \bar{a}\bar{f}}{\bar{a}\bar{g} - \bar{b}\bar{d}}\right] p = -H_2 \qquad [9]$$

and the transverse shearing force from

$$Q_i = H_i \cos \alpha_i \pm \frac{pR_i}{2} \sin \alpha_i \qquad [10]$$

where

$$\bar{a} = a_1 + a_2;\ \bar{b} = b_1 - b_2;\ \bar{c} = c_1 + c_2$$

$$\bar{d} = d_1 - d_2;\ \bar{f} = f_1 - f_2;\ \bar{g} = g_1 + g_2$$

The quantities a_1, a_2, b_1, b_2 . . . are edge coefficients defined for conical and cylindrical shells as

$$a_i = -\frac{U^3}{E}\sqrt{\frac{2R_i}{h_i^5 \cos \alpha_i}}$$

$$b_i = +\frac{U^2 R_i}{E h_i^2}$$

$$c_i = \pm \frac{U^2}{2E} \frac{R_i^2 \tan \alpha_i}{h_i^2} \mp \frac{3R_i}{2Eh_i} \frac{\tan \alpha_i}{\cos \alpha_i} \qquad [11]$$

$$d_i = +\frac{U^2 R_i}{E h_i^2}$$

$$f_i = \mp \frac{U}{E}\sqrt{\frac{R_i^5 \sin^2 \alpha_i}{2 h_i^3 \cos \alpha_i}} + \frac{\left(1 - \frac{\nu}{2}\right)}{E} \frac{R_i^2}{h_i \cos \alpha_i}$$

and

$$g_i = -\frac{\sqrt{2}\ U}{E}\sqrt{\frac{R_i^3}{h_i^3}}\ \cos\alpha_i$$

where

$$U = \sqrt[4]{12\ (1-\nu^2)}$$

These edge coefficients are functions of the shell geometries and material properties only and are independent of the type of intersection. Since the coordinate x is measured from the intersection (Figure 4), the signs of the coefficients a_i, b_i, and c_i differ from those given in Reference 5 where x is measured from the cone apex. The upper signs in Equations [10] and [11] apply to the large-diameter end of a cone, and the lower ones to the small-diameter end of a truncated cone. It should be noted that those terms in Equations [11] with alternate signs vanish for a cylinder since $\alpha = 0$.

Thus, after the appropriate edge coefficients have been determined from Equations [11] the edge moments and shears at the unreinforced intersection of any combination of two cylindrical or conical shells may be found from Equations [9] and [10].

For the particular case of the intersection of the large-diameter end of a truncated cone ($i = 1$) with a cylinder ($i = 2$) of the same shell thickness ($h_1 = h_2 = h$), Equations [9] and [10] reduce to the following:

$$M_1 = \frac{p \sin\alpha \sqrt{R_1^3\, h}}{\sqrt{8}\ U\ (\cos\alpha + \sqrt{\cos\alpha})}\left[1 - \frac{3h}{U^2 R_1 \cos\alpha}\right] = M_2$$

$$H_1 = -\frac{pR_1 \sin\alpha}{2\ (\cos\alpha + \sqrt{\cos\alpha})}\left[1 - \frac{\sqrt{2}\ (1 - \frac{\nu}{2})\ (1 - \cos\alpha)}{U \sin\alpha}\sqrt{\frac{h}{R_1 \cos\alpha}}\right] = -H_2 = -Q_2$$

[12]

$$Q_1 = H_1 \cos\alpha + \frac{pR_1}{2}\sin\alpha$$

where R_1 is the radius of the larger end (base circle) of the cone.

Another special case is that of the intersection of the small-diameter end of a truncated cone ($i = 1$) with a cylinder ($i = 2$) of the same shell thickness. Here, Equations [9] and [10] become:

$$M_1 = \frac{p \sin\alpha \sqrt{R_1'^3 h}}{\sqrt{8}\, U (\cos\alpha + \sqrt{\cos\alpha})} \left[1 + \frac{3h}{U^2 R_1' \cos\alpha}\right] = M_2$$

$$H_1 = \frac{pR_1' \sin\alpha}{2(\cos\alpha + \sqrt{\cos\alpha})} \left[1 + \frac{\sqrt{2}(1 - \frac{\nu}{2})(1 - \cos\alpha)}{U \sin\alpha} \sqrt{\frac{h}{R_1' \cos\alpha}}\right] = -H_2 = -Q_2 \qquad [13]$$

$$Q_1 = H_1 \cos\alpha - \frac{pR_1'}{2} \sin\alpha$$

where R_1' is the radius of the smaller end (frustrum circle) of the cone.

CASE B: CONICAL OR CYLINDRICAL SHELLS WITH CLAMPED EDGES, SUBJECT TO EXTERNAL HYDROSTATIC PRESSURE

When cone-cylinder intersections are reinforced by very heavy bulkheads, reasonably accurate solutions may be obtained by treating each component shell separately and assuming that the edges of each shell are rigidly fixed, i.e., zero radial displacement and zero rotation. The resulting bending moments, radial shearing forces, and transverse shearing forces for this case are, respectively,

$$M = \frac{pRh(1 - \frac{\nu}{2})}{U^2 \cos\alpha} \mp \frac{3p}{\sqrt{2}\, U^3} \sqrt{\frac{Rh^3 \tan^2\alpha}{\cos\alpha}}$$

$$H = \mp \frac{pR}{2} \tan\alpha \mp \frac{3ph \tan\alpha}{2U^2 \cos\alpha} + \frac{\sqrt{2}\, p(1 - \frac{\nu}{2})}{U} \sqrt{\frac{Rh}{\cos^3\alpha}} \qquad [14]$$

$$Q = H \cos\alpha \pm \frac{pR}{2} \sin\alpha$$

where the upper sign in each expression together with $R = R_1$ applies to the large-diameter end of a truncated cone and the lower sign together with $R = R_1'$ applies to the small-diameter end. These same equations may be used to determine the fixed-ended moment and shear for a cylindrical shell by setting $\alpha = 0$. It should be noted that the terms with alternative plus and minus signs will vanish for the case of the cylinder.

CASE C: INTERSECTION OF CONICAL AND CYLINDRICAL SHELLS REINFORCED BY A STIFFENER OF FINITE RIGIDITY, SUBJECT TO EXTERNAL HYDROSTATIC PRESSURE

A general composite structure, that of two intersecting cones, covered under this case, is shown schematically in Figure 5.

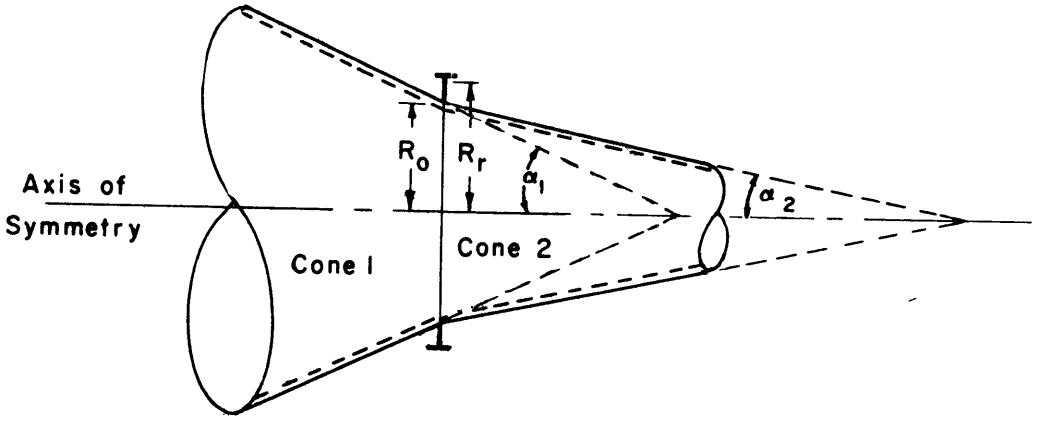

Figure 5 - Reinforced Cone-Cone Juncture

Particular cases of interest to the pressure-vessel designer which are specializations of this somewhat general case are: the reinforced intersection of the large-diameter end of a cone with a cylinder, that of the small-diameter end of a truncated cone with another cylinder, that of two cylinders, that of the large-diameter ends of two cones, and that of the small-diameter ends of two truncated cones.

For all these cases, the simplifying assumption is made that the two shell elements and the reinforcing ring have line contact around the circumference at their common juncture. A more refined analysis including the effects of a finite-width intersection is presented in the next section.

The discontinuity shears and moments acting on the edges of the two shell elements identified by the subscripts $i = 1$ and $i = 2$ as in Figure 5 may be determined by solving the following set of four simultaneous algebraic equations. These equations result from satisfying conditions of continuity of radial displacements and angular rotations of the three intersecting elements at their common juncture, and force and moment equilibrium.

$$
\begin{aligned}
&d_1 M_1 + \left(g_1 - \frac{R_0}{R_r}\, k_a\right) H_1 - k_a H_2 \frac{R_0}{R_r} = -f_1 p \\
&d_2 M_2 - k_a H_1 \frac{R_0}{R_r} + \left(g_2 - k_a \frac{R_0}{R_r}\right) H_2 = -f_2 p \qquad [15] \\
&\left(a_1 - k_b \frac{R_0}{R_r}\right) M_1 + \frac{R_0}{R_r}\, k_b M_2 + b_1 H_1 = -c_1 p
\end{aligned}
$$

$$\frac{R_0}{R_r} k_b M_1 + \left(a_2 - k_b \frac{R_0}{R_r} \right) M_2 + b_2 H_2 = - c_2 p$$

where

$$k_a = \frac{R_r^2}{EA_r} \; ; \quad k_b = \frac{R_r^2}{EI_r}$$

and A_r is the cross-sectional area of the ring stiffener,

I_r is the moment of inertia of the ring cross section about the radial axis through its center of gravity,

R_r is the radius to the center of gravity of the ring cross section from the axis of symmetry, and

E is Young's modulus for the ring material.

As has already been mentioned, the general Equations [15] may be applied to the reinforced intersection of any combination of two conical or cylindrical shells simply by computing the appropriate edge coefficients (a_1, a_2, b_1, b_2, etc.) for each component shell from Equations [11]. The procedure for getting these coefficients is identical to that for the unreinforced intersection problem, Case A. The transverse shearing force Q_i may be determined as before from Equation [10].

CASE D: EFFECT OF A HEAVY FORGED-RING TYPE STIFFENER UPON THE INTERSECTION DEFORMATIONS

In Case C where various reinforced intersections were considered, it was assumed that the stiffening rings were very narrow so that there was practically line contact around the circumference at the common juncture of the three elements—the ring and the two axisymmetric shells. Consequently, the axial rotations θ_i and radial displacements $\bar{w}_i$ of the two component shells and the stiffening ring were considered to be equal at the common juncture. This is a valid assumption provided the stiffening ring actually is very narrow as in the case of a deep slender rectangular or "Tee" cross section attached at the web as shown in Figure 5.

If, however, the stiffening ring has a thick web or a wide faying flange, or if the intersection includes a heavy forged ring as is common in submarine pressure-hull design, then the juncture effectively consists of the two shell edges with a reinforcement of finite dimensions between them; see Figure 6. Although the lines of action of the axial membrane forces of the component shells may intersect at a common point on the centroidal z-axis of the forged ring and stiffener, eccentricities in the radial as well as in the axial direction may arise where the edges of the shells meet the forging. The effects of these eccentricities on the discontinuity moments and shearing forces, which may be significant, are taken into consideration in the following extended analysis of the boundary conditions. Here, as before, any secondary bending of the juncture ring in the meridional plane is neglected.

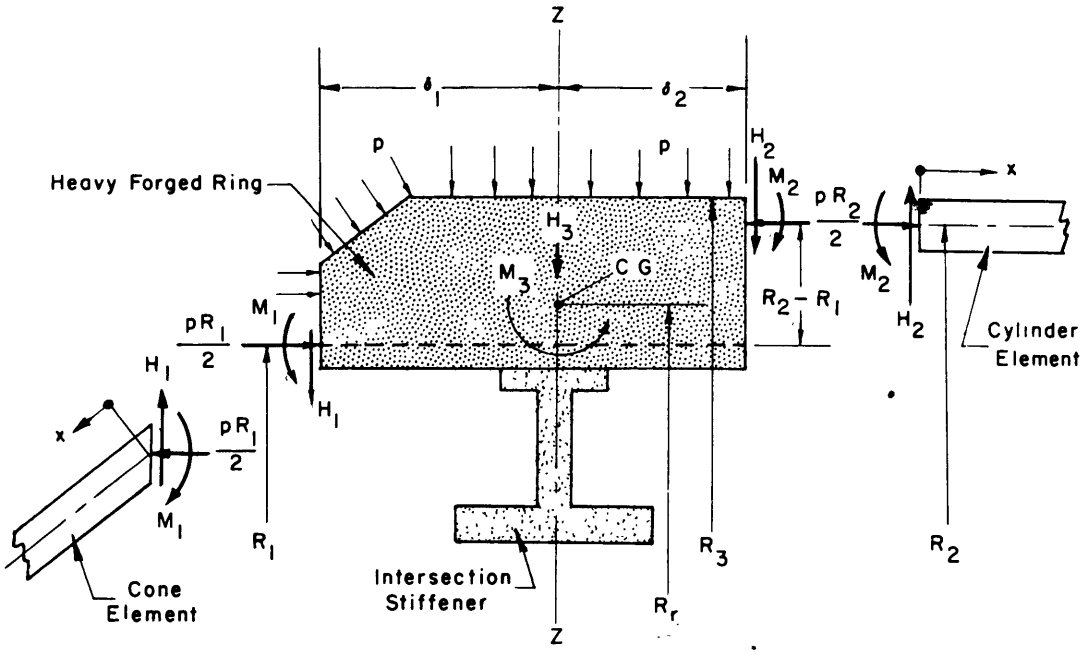

Figure 6 - Notation for Reinforcement at Cone-Cylinder Juncture

The new juncture conditions are as follows:

Force and moment equilibrium require,

$$H_3 = \frac{R_1}{R_r} H_1 + \frac{R_2}{R_r} H_2 + p(\delta_1 + \delta_2)\frac{R_3}{R_r}$$

$$M_3 = \frac{R_1}{R_r} M_1 - \frac{R_2}{R_r} M_2 + \frac{R_1}{R_r} \delta_1 H_1 - \frac{R_2}{R_r} \delta_2 H_2 + \frac{p}{8R_r}(R_2 - R_1)(R_2 + R_1)^2 + \frac{p}{2}(\delta_1^2 - \delta_2^2)\frac{R_3}{R_r} \qquad [16]$$

while continuity of structure requires,

$$\bar{w}_1 = \bar{w}_3 + \delta_1 \theta_3$$

$$\bar{w}_2 = \bar{w}_3 - \delta_2 \theta_3 \qquad [17]$$

$$\theta_1 = \theta_3 = -\theta_2$$

where the rotation θ_3 and radial displacement $\bar{w}_3$ of the juncture ring are given in Reference 5 to be

$$\theta_3 = k_b M_3 = k_b \left[\frac{R_1}{R_r} M_1 - \frac{R_2}{R_r} M_2 + \frac{R_1}{R_r} \delta_1 H_1 - \frac{R_2}{R_r} \delta_2 H_2 + \frac{p}{8R_r} (R_2 - R_1)(R_2 + R_1)^2 \right.$$

$$\left. + \frac{p}{2} (\delta_1^2 - \delta_2^2) \frac{R_3}{R_r} \right] \qquad [18]$$

$$\bar{w}_3 = k_a H_3 = k_a \left[\frac{R_1}{R_r} H_1 + \frac{R_2}{R_r} H_2 + p (\delta_1 + \delta_2) \frac{R_3}{R_r} \right]$$

where

$$k_a = \frac{R_r^2}{EA_r} \qquad \text{and} \qquad k_b = \frac{R_r^2}{EI_r}$$

from the elementary thin-ring analysis. Here A_r is the cross-sectional area and I_r is the moment of inertia about the z-axis of the composite reinforcement shown shaded in Figure 6.

The total rotations and radial displacements at the edge of each component shell for combined loading are obtained by superposition:

$$\begin{aligned} \theta_1 &= a_1 M_1 + b_1 H_1 + c_1 p \\ \bar{w}_1 &= d_1 M_1 + g_1 H_1 + f_1 p \\ \theta_2 &= a_2 M_2 + b_2 H_2 + c_2 p \\ \bar{w}_2 &= d_2 M_2 + g_2 H_2 + f_2 p \end{aligned} \qquad [19]$$

where the edge coefficients a_1, a_2, b_1, b_2, etc. are defined by Equations [11] as before.

The four continuity conditions [17] together with Equations [18] and [19] lead to the following system of four simultaneous algebraic equations for the unknown discontinuity moments and shears M_1, M_2, H_1, and H_2:

$$\left(d_1 - \delta_1 k_b \frac{R_1}{R_r} \right) M_1 + \delta_1 k_b \frac{R_2}{R_r} M_2 + \left(g_1 - k_a \frac{R_1}{R_r} - \delta_1^2 k_b \frac{R_1}{R_r} \right) H_1$$

$$+ \left(\delta_1 \delta_2 k_b \frac{R_2}{R_r} - k_a \frac{R_2}{R_r} \right) H_2 = \left[-f_1 + (\delta_1 + \delta_2) k_a \frac{R_3}{R_r} \right. \qquad [20]$$

$$\left. + \frac{\delta_1}{8R_r} k_b (R_2 - R_1)(R_2 + R_1)^2 + \frac{\delta_1}{2} k_b (\delta_1^2 - \delta_2^2) \frac{R_3}{R_r} \right] p$$

$$\delta_2 k_b \frac{R_1}{R_r} M_1 + \left(d_2 - \delta_2 k_b \frac{R_2}{R_r}\right) M_2 + \left(\delta_1 \delta_2 k_b \frac{R_1}{R_r} - k_a \frac{R_1}{R_r}\right) H_1$$

$$+ \left(g_2 - k_a \frac{R_2}{R_r} - \delta_2^2 k_b \frac{R_2}{R_r}\right) H_2 = \left[-f_2 + (\delta_1 + \delta_2) k_a \frac{R_3}{R_r}\right.$$

$$\left. - \frac{\delta_2}{8R_r} k_b (R_2 - R_1)(R_2 + R_1)^2 - \frac{\delta_2}{2} k_b (\delta_1^2 - \delta_2^2) \frac{R_3}{R_r}\right] p$$

$$\left(a_1 - k_b \frac{R_1}{R_r}\right) M_1 + k_b \frac{R_2}{R_r} M_2 + \left(b_1 - \delta_1 k_b \frac{R_1}{R_r}\right) H_1 + \delta_2 k_b \frac{R_2}{R_r} H_2 \qquad [20]$$

$$= \left[-c_1 + \frac{k_b}{8R_r}(R_2 - R_1)(R_2 + R_1)^2 + \frac{k_b}{2}(\delta_1^2 - \delta_2^2) \frac{R_3}{R_r}\right] p$$

$$k_b \frac{R_1}{R_r} M_1 + \left(a_2 - k_b \frac{R_2}{R_r}\right) M_2 + \delta_1 k_b \frac{R_1}{R_r} H_1 + \left(b_2 - \delta_2 k_b \frac{R_2}{R_r}\right) H_2$$

$$= \left[-c_2 - \frac{k_b}{8R_r}(R_2 - R_1)(R_2 + R_1)^2 - \frac{k_b}{2}(\delta_1^2 - \delta_2^2) \frac{R_3}{R_r}\right] p$$

Thus, for all the examples considered under Case C, if the reinforcing rings have faying webs or flanges of appreciable width or if the intersection includes a heavy forged ring as shown in Figure 5, Equations [20] should be used instead of [15]. Any contiguous piece of shell material in contact with the faying flange should be included when computing A_r and I_r.

APPLICABILITY OF METHOD

The range of applicability of the methods in this report was determined by comparing the edge coefficients with those of the exact solution of Reference 6. The expressions for determining the edge forces and moments and the stresses and strains are derived from the

transverse deflection function and its derivatives. The higher derivatives of w, at least through the third, will be as valid as w itself, since derivatives up to the third were used in determining the constants of integration. Therefore, the accuracy of the computed stresses and strains should be about equal to that of the deflection function. The edge coefficients are found directly from w and its first derivative, evaluated at the shell edge ($x = 0$) so that the errors in the entire analysis should be of the same order of magnitude as those in the edge coefficients.

The edge coefficients that follow from the analysis of the report are almost identically equal to those obtained by setting the special Ω functions, which appear as multiplying factors in the coefficients of the exact solution of Reference 6, equal to unity. The exceptions are that the third terms in the equations for c_i and f_i are not present in the approximate coefficients of this report. However, these omitted terms are generally negligible compared to the other terms if α is not nearly equal to $\pi/2$. An estimate of the maximum error in each of the approximate edge coefficients may be made in terms of the special Ω functions, appearing in Reference 6, of the dimensionless parameter ξ, where

$$\xi = 2 \sqrt[4]{\frac{12\,(1-\nu^2)\,R^2\cos^2\alpha}{h^2\sin^4\alpha}}$$

If ξ is restricted to values of 10 or more for a conical shell made of steel ($\nu = 0.3$), the maximum error in any one of the edge coefficients computed from Equation [11] of this report would be about 10.5 percent for the large-diameter end and about 6.9 percent for the small-diameter end of the cone. If ξ is restricted to values of 20 or more, the maximum errors would be about 4.8 percent and 3.8 percent, respectively. The inequality $\xi \geq 10$ corresponds to

$$\frac{2R\cos\alpha}{h\sin^2\alpha} \geq 15$$

and $\xi \geq 20$ to

$$\frac{2R\cos\alpha}{h\sin^2\alpha} \geq 60$$

The analysis presented in this report is also based upon the assumption that the axisymmetric shell elements are of semi-infinite length so that there is no interaction between discontinuity forces and moments arising at adjacent ends. From an examination of Figures 2 and 3 it can be seen that this condition is satified if $\beta_i l$ for either end is greater than or equal to 3.0 (where l is the length of shell between discontinuities). If the value of $\beta_i l$ is less than 6.0, then the discontinuity stresses and strains from each end will overlap through a portion of the shell and they should then be superimposed. This linear superposition may

be done graphically as in the example of Appendix A.

The discontinuity bending moments and shearing forces which arise at the juncture of any two shells of revolution may be found from Equations [9], [15], or [20] providing the appropriate edge coefficients for the component shells are used. In Reference 2, Timoshenko gives an approximate method for analyzing the stresses in spherical shells in which he simplifies the problem by replacing the portion of the shell near the edge by a tangent conical shell and, in turn, treating this as an "equivalent cylinder." In this particular case, the edge coefficients a_i, b_i, d_i, and g_i as given by Equation [11] can be used directly, but the membrane (second) terms of c_i and f_i for a spherical shell should be derived. Similarly, Equations [1] through [5] can be used to compute the stresses and strains in such a shell except that the membrane terms appearing there, those terms containing the pressure p, should be replaced with those derived for a spherical shell. This same procedure for analyzing discontinuity stresses may be extended to any other shells of revolution, i.e., ellipsoidal, torispherical, tori-conical, provided the slope and change in slope at the edges are not too great.

Although the results presented herein lead to a rapid method for computing elastic stresses, which at the same time have been verified by experiment, no attempt is made in this report to establish a criterion for allowable stress in design. The application of these results to a design process is subject to the skill and judgment of the engineering designer.

ACKNOWLEDGMENTS

The authors are greatly indebted to Dr. C.E. Taylor, who initiated the work included in the present report.

Much helpful advice and criticism was contributed by Dr. E. Wenk during the writing of the report.

The computations were ably carried out by Mrs. M.R. Overby.

APPENDIX A

NUMERICAL EXAMPLE

The methods described herein for computing the edge moments and shearing forces and the resulting stresses and strains in the vicinity of an intersection reinforced by a ring of finite dimensions will be applied to a specific model tested at the Taylor Model Basin as an illustration. This model consists of two cylindrical shells of different diameters joined by a conical transition section. Both cone-cylinder intersections were reinforced with stiffening rings of finite dimensions. The dimensions, including details of the cross section of the large cone-cylinder intersection are shown in Figure 7.

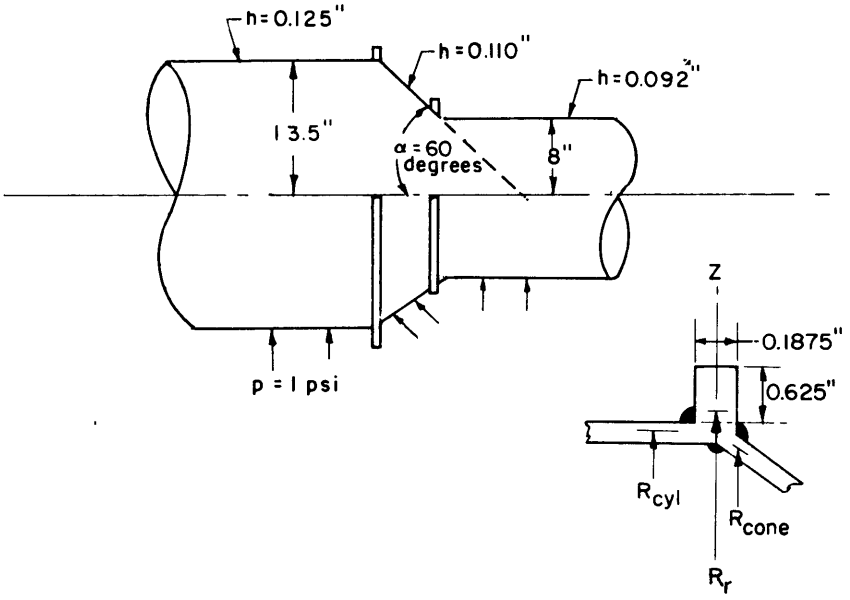

Figure 7 - Schematic Drawing of Illustrative Model

The analysis of the large-diameter intersection will be demonstrated in detail. An examination of the cross section of the juncture shows the effective stiffening ring to have an appreciable width which is estimated to be 0.36 in. (including effective weld material); therefore, $\delta_1 \approx \delta_2 \approx 0.18$ in. The radii of the two shells at the juncture and the radius to the neutral axis of the ring are very nearly equal so it is assumed that

$$\frac{R_1}{R_r} \approx \frac{R_2}{R_r} \approx \frac{R_3}{R_r} \approx 1.0$$

and

$$R_2 - R_1 \approx 0$$

The moments and shearing forces, M_1, M_2, H_1, and H_2 will be determined from Equations [20]. The subscript "1" will be assigned to the cone, and "2" to the cylinder. Note that every term in Equation [20] contains Young's modulus E in the denominator. Since all the component parts of the juncture are made of the same material (steel, for which $E = 30 \times 10^6$ psi), all equations may be multiplied by E to simplify the computation. Edge coefficients (multiplied by E) are first computed for both shells from Equations [11]. Then the cross-sectional area A_r and moment of inertia I_r (about axis $z - z$) of the effective ring are computed, and the quantities Ek_a and Ek_b are determined from Equations [18]. The values thus determined are substituted into Equations [20] which are then solved numerically, giving:

$$M_1 = 2.16056$$
$$M_2 = 0.739266$$
$$H_1 = -5.69747$$
$$H_2 = 2.27055$$

From Equation [10]:

$$Q_1 = 2.99694$$
$$Q_2 = H_2 = 2.27055$$

Note that a large number of significant figures are carried here and in the following calculations. This is believed necessary because of the many numerical operations that are performed on each quantity.

With these values for M_1, M_2, Q_1, and Q_2 and the geometric and material properties of the shells, the stresses and strains in the large cylinder and in the cone as the result of the discontinuities arising from the juncture with the stiffening ring may be determined from Equations [1] through [5]. Membrane stresses and strains (due to pressure alone) are included in these expressions. When all these stresses and strains are to be found for a large number of values of x, the computations are rather tedious, so a calculation sheet has been devised which facilitates the work somewhat. This sheet, filled in for the large-diameter end of the cone of the model under discussion, is shown in Table 2. The numbers and expressions in bold-face type are permanent figures on the sheet. Similar calculation sheets for the large-diameter cylinder, the small-diameter cylinder and the small-diameter end of the cone are required to obtain a complete stress and strain distribution. Note that on the sample calculation sheet the procedure was not derived from Equations [1] through [5], but directly from the expressions appearing in Appendix C. This amounts to an algebraic rearrangement of Equations [1] through [5] which was found more advantageous in cases where a large number of calculations are required for all the stresses and strains.

The circumferential strain distribution as a function of distance from each intersection are shown as solid lines for the two cylinder components and as broken lines for the cone in

TABLE 2

Calculation Sheet for Computing Stresses and Strains at Large-Diameter End of Cone in Illustrative Example

1 $\beta_i x$	2 x	3 $x \sin \alpha_i$	4* $R_i \pm$ ③	5 $\psi(\beta x)$	6 $\zeta(\beta x)$	7 $\frac{2\beta_i M_i \tan \alpha_i}{h_i} \times$ ⑥	8 $\frac{Q_i \tan \alpha_i}{h_i} \times$ ⑤	9 ⑦ + ⑧	10 $\frac{-1}{2h_i \cos \alpha_i} \times$ ④	11 ⑨ + ⑩	12 $\theta(\beta x)$
0	0	0	13.500	1.0000	0	0	47.18	47.18	−122.72	− 75.53	1.0000
0.3	0.4022	0.3483	13.151	0.4888	0.2189	11.10	23.06	34.17	−119.56	− 85.38	0.7077
0.6	0.8044	0.6866	12.803	0.1431	0.3099	15.72	6.75	22.47	−116.39	− 93.91	0.4530
1.0	1.3407	1.1610	12.338	−0.1108	0.3096	15.71	− 5.22	10.48	−112.17	−101.68	0.1988
1.4	1.8770	1.6255	11.874	−0.2011	0.2430	12.33	− 9.48	2.84	−107.94	−105.10	0.0419
2.0	2.6814	2.3221	11.177	−0.1794	0.1230	6.24	− 8.46	− 2.22	−101.61	−103.84	−0.0563
3.0	4.0221	3.4832	10.016	−0.0563	0.0071	0.36	2.65	− 2.29	− 91.06	− 93.35	−0.0493
4.0	5.3628	4.6443	8.855	0.0019	−0.0139	− 0.70	0.08	− 0.61	− 80.50	− 81.12	−0.0120
5.0	6.7035	5.8054	7.694	0.0084	− 0.0065	− 0.32	0.39	+ 0.06	− 69.95	− 69.88	0.0019

13 $\frac{U^2 Q_i}{h_i^2 \beta_i} \times$ ⑫	14 $-\frac{U^2 M_i}{h_i^2} \times$ ⑤	15 $\nu \times$ ⑨	16 $\frac{-1}{h_i \cos \alpha_i} \times$ ④	17 ⑬ + ⑭ + ⑮ + ⑯	18 $\phi(\beta x)$	19 $\frac{6M_i}{h_i^2} \times$ ⑱	20 $-\frac{6Q_i}{h_i^2 \beta_i} \times$ ⑥	21 ⑲ + ⑳	22 $\nu \times$ ㉑	23 $-\nu/E \times$ ⑪ $\times 10^6$	24 $1/E \times$ ⑰ $\times 10^6$
1097.33	−590.05	14.15	−245.45	275.98	1.0000	1071.35	0	1071.35	321.40	0.75	9.19
776.58	−288.41	10.25	−239.12	259.29	0.9267	992.82	−436.14	556.68	167.00	0.85	8.64
497.09	− 84.43	6.74	−232.78	186.61	0.7628	817.22	−617.45	199.77	59.93	0.93	6.22
218.15	+ 65.37	3.14	−224.34	62.33	0.5083	544.56	−616.85	− 72.28	− 21.68	1.01	2.07
45.97	+118.65	0.85	−215.89	− 50.40	0.2849	305.22	−484.15	− 178.92	− 53.67	1.05	−1.68
− 61.78	+105.85	− 0.66	−203.23	−159.82	0.0667	71.45	−245.06	− 173.60	− 52.08	1.03	−5.32
− 54.09	+ 33.22	− 0.68	−182.12	−203.68	− 0.0423	− 45.31	− 14.14	− 59.46	− 17.83	0.93	−6.78
− 13.16	− 1.12	− 0.18	−161.01	−175.48	− 0.0253	− 27.64	27.69	0.05	0.01	0.81	−5.84
2.08	2.08	0.01	−139.90	−142.75	− 0.0046	− 4.92	12.95	8.02	2.40	0.69	−4.75

25 $\epsilon_\phi \times 10^6$ ㉓ + ㉔	26 $-\nu/E \times$ ⑰ $\times 10^6$	27 $1/E \times$ ⑪ $\times 10^6$	28 $\frac{1-\nu^2}{E} \times$ ㉑ $\times 10^6$	29 $\epsilon_{x\ \text{ext.}} \times 10^6$ ㉖ + ㉗ + ㉘	30 $\epsilon_{x\ \text{int.}} \times 10^6$ ㉖ + ㉗ − ㉘	31 $\sigma_{x\ \text{ext.}}$ ⑪ + ㉑	32 $\sigma_{x\ \text{int.}}$ ⑪ − ㉑	33 $\sigma_{\phi\ \text{ext.}}$ ⑰ + ㉒	34 $\sigma_{\phi\ \text{int.}}$ ⑰ − ㉒		
9.95	−2.75	−2.51	32.49	27.21	−37.77	995.81	− 1146.89	597.39	− 45.41		
9.49	−2.59	−2.84	16.88	11.44	−22.32	471.29	− 642.06	426.30	+ 92.29		
7.15	−1.86	−3.13	6.05	1.06	−11.05	105.86	− 293.69	246.54	+126.68		
3.09	−0.62	−3.38	− 2.19	− 6.20	− 1.82	−173.97	− 29.40	40.64	+ 84.01		
−0.62	0.50	−3.50	− 5.42	− 8.42	+ 2.42	−284.03	+ 73.82	−104.08	+ 3.27		
−4.28	1.59	−3.46	− 5.26	− 7.12	+ 3.40	−277.44	+ 69.76	−211.90	−107.74		
−5.85	2.03	−3.11	− 1.80	− 2.87	+ 0.72	−152.82	− 33.89	−221.52	−185.85		
−5.03	1.75	−2.70	0.00	− 0.94	− 0.95	− 81.06	− 81.17	−175.46	−175.50		
−4.05	1.42	−2.32	0.24	− 0.65	− 1.14	− 61.86	− 77.90	−140.34	−145.15		

	M_i	2.16056	$\tan \alpha_i$	1.73205	$\frac{2\beta_i M_i \tan \alpha_i}{h_i}$	50.748	$\frac{U^2 Q_i}{h_i^2 \beta_i}$	1097.338	$\frac{6M_i}{h_i^2}$	1071.35	
	H_i	− 5.69747	Q_i	2.99694	$\frac{Q_i \tan \alpha_i}{h_i}$	47.189	$\frac{U^2 M_i}{h_i^2}$	590.054	$\frac{6Q_i}{h_i^2 \beta_i}$	1992.41	
	α_i	60 degrees	β_i	0.745870	$\frac{1}{2h_i \cos \alpha_i}$	9.09090	$\frac{1}{h_i \cos \alpha_i}$	18.1818	$\frac{1-\nu^2}{E} \times 10^6$	= 0.030333	
	$\sin \alpha_i$	0.866025	R_i	13.500							
	$\cos \alpha_i$	0.500000	h_i	0.110							

*The plus sign applies to the small-diameter end of a truncated cone and the minus sign to the large-diameter end.

Figure 8. The circumferential membrane distribution for the cone, represented by the first term of Equation [5], is also shown. It is seen that the discontinuity effects from both intersections exist throughout most of the conical shell and overlap with each other, that is, the circumferential discontinuity strains indicated by the broken curves differ from the membrane strain throughout a large portion of the cone. The total circumferential strain at any point in the conical shell then is the algebraic sum of the discontinuity strains from both intersections and the membrane strain. This superposition was done graphically in Figure 8 and the resulting distribution is shown as the solid line labeled $\epsilon_{\phi_{\text{Total}}}$. The broken-line curve labeled 1 was found from the analysis of the large end of the cone and that labeled 2 from the analysis of the small end. The difference between the ordinates of curve 2 and the membrane line were then added to those of curve 1 to obtain $\epsilon_{\phi_{\text{Total}}}$.

A similar procedure was followed in determining the distribution of longitudinal strain on both the external and internal surfaces of the shell elements. The longitudinal strain distributions for this example are shown in Figure 9. For clarity of the curves, the component strains (strains from each intersection and the membrane distribution) are not shown. Note that the total strains and also stresses thus found are for an external pressure of 1 psi; i.e., they are essentially strain and stress sensitivity distributions.

The technique indicated by the results of Figures 8 and 9 of this report for linearly superposing the discontinuity and membrane effects can be used for short shells provided the length l between adjacent edgesis such that $\beta_i l \geq 3.0$; this has already been discussed under "Applicability of Method." For cases where $\beta_i l < 3.0$ the discontinuity forces and moments at one edge of the shell may influence those at an adjacent edge and vice versa, so that in such instances this method of superposition may still be used but the resulting distributions would be questionable. An analysis which considers this interaction and which may prove convenient in practical application is given in Reference 8.

Experimental strain data have also been plotted on Figures 8 and 9 for comparison with the theoretical distributions determined by the analysis given herein. It is seen from these plots that the agreement between theory and experiment for this particular case is very good and certainly falls within the limits of experimental error. The agreement is considered fortuitous, and this one example does not constitute any extensive verification of the simplified cone analysis presented. This model is one of a series of six such models which have already been tested at the Taylor Model Basin. The experimental strain data obtained from the complete program will be used to check further the validity of the simplified cone analysis developed in this report. These additional results will be forthcoming in a Taylor Model Basin report.

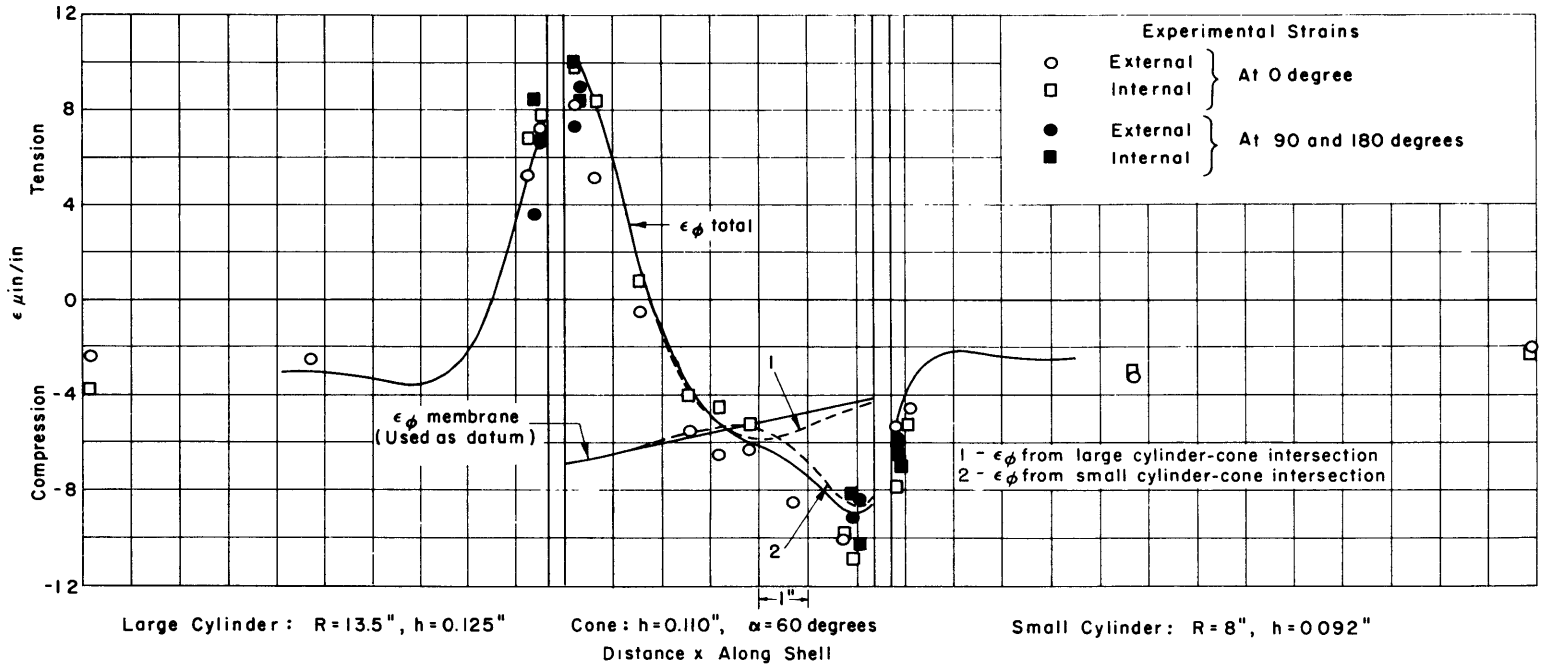

Figure 8 - Theoretical and Experimental Circumferential Strains in Illustrative Model for External Hydrostatic Pressure of 1 PSI

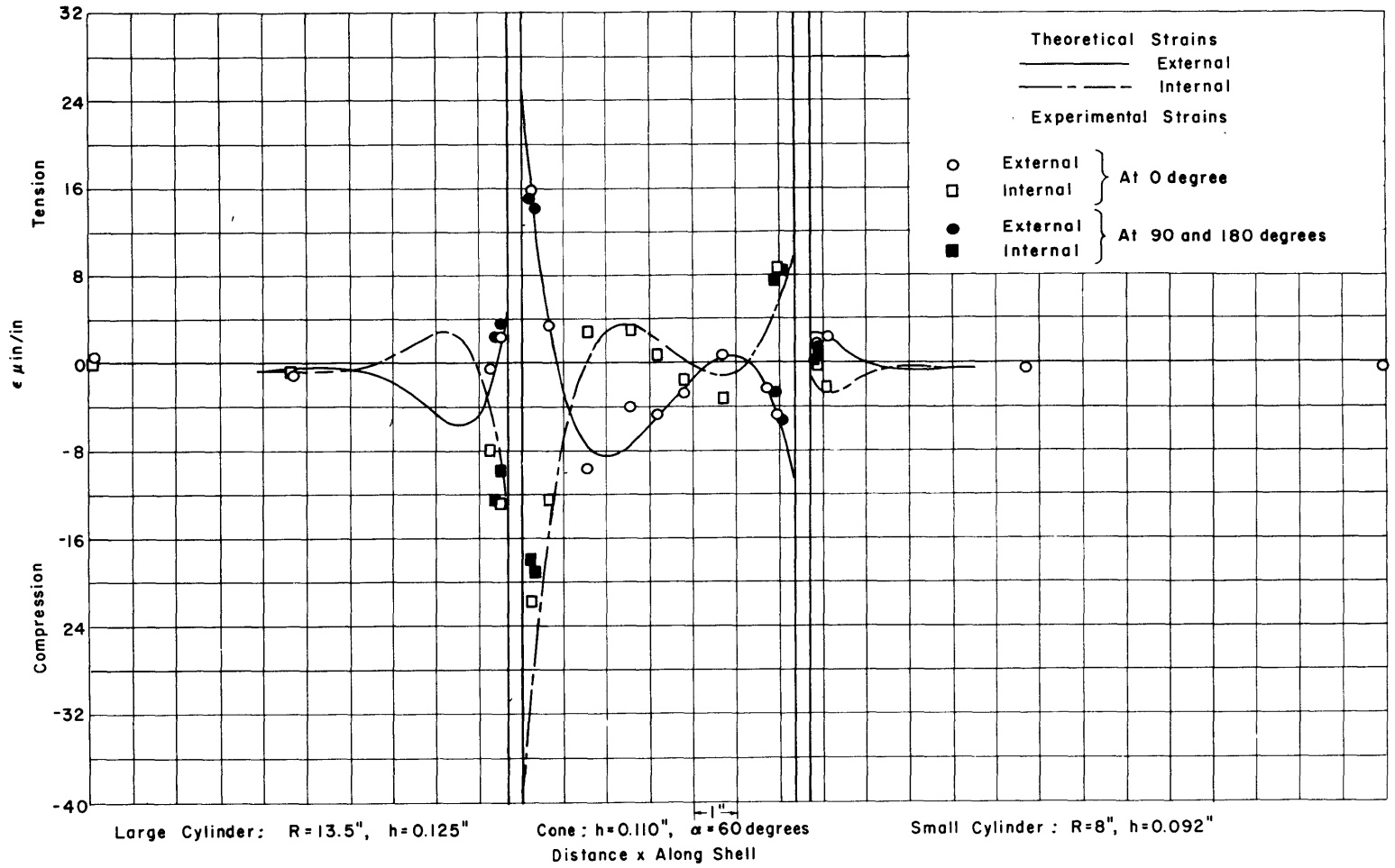

Figure 9 - Theoretical and Experimental Longitudinal Strains on External and Internal Surfaces of Illustrative Model for External Hydrostatic Pressure of 1 PSI

APPENDIX B

GECKELER APPROXIMATION FOR CONICAL SHELLS

From considerations of equilibrium of a shell element, Dubois[3] established by standard elastic analysis an expression for the transverse displacement w of a thin conical shell in terms of a fourth-order differential equation. The homogeneous form of this equation is

$$y^2 \frac{d^4 w}{dy^4} + 2y \frac{d^3 w}{dy^3} - 2 \frac{d^2 w}{dy^2} + \frac{12 (1 - \nu^2)}{h^2 \tan^2 \alpha} w = 0 \qquad [B.1]$$

where y is the meridional distance along a cone element measured from the apex.

Solutions of Equation [B.1] are considered to be very accurate but usually require far too much computational time to be practical. Hence, resort is often made to approximate methods of the type discussed below. Taylor and Wenk in Reference 6 have found solutions to the complete Equation [B.1] in terms of Bessel functions of the first and second kind, both of second order.

The radius R for any point on the cone is (Figure 1)

$$R = y \sin \alpha \qquad [B.2]$$

If the y's, which are coefficients of the derivatives in Equation [B.1], are eliminated by using [B.2], and if [B.1] is then multiplied by $\sin^2 \alpha$, the following results:

$$R^2 \frac{d^4 w}{dy^4} + 2R \frac{d^3 w}{dy^3} \sin \alpha - 2 \frac{d^2 w}{dy^2} \sin^2 \alpha + \frac{12 (1 - \nu^2) \cos^2 \alpha}{h^2} w = 0 \qquad [B.3]$$

It has been shown in Reference 5 by order-of-magnitude considerations that, for the range of parameters of interest to pressure-vessel designers,

$$\left| R^2 \frac{d^4 w}{dy^4} \right|_{max} >> \left| 2R \frac{d^3 w}{dy^3} \sin \alpha \right|_{max} >> \left| 2 \frac{d^2 w}{dy^2} \sin^2 \alpha \right|_{max} >> \left| \frac{2}{R} \frac{dw}{dy} \sin^3 \alpha \right|_{max} \qquad [B.4]$$

i.e., the second- and third-order terms appearing in the complete Equation [B.3] may be neglected in comparison with the fourth-order one. Wenk and Taylor in Reference 5 carried out the first approximation, that of neglecting the second-order term only, and obtained a solution for the transverse displacement w in terms of Bessel functions of the first and second kind, both of zero order. They indicate that from the inequalities [B.4] the original differential equation could be further simplified if the third-order term is also neglected. The analysis of the present report is based on this second approximation.

Further, the discontinuity bending stresses are very local and damp out rapidly away from the juncture region of any two intersecting shells. Hence it is sufficiently accurate to

treat the radius R appearing in Equation [B.3] as constant and equal to R_0, the radius at the edge of the component shell, in determining these local effects. Geckeler[2] proposed approximations of this type in dealing with such local bending effects in thin shells; thus the so-called "Geckeler approximation" for conical shells reduces to the integration of the equation:

$$\frac{d^4w}{dy^4} + \frac{12\,(1-\nu^2)\cos^2\alpha}{h^2R_0^2}\,w = 0 \qquad [B.5]$$

As may be seen from Figure 1, the distance x from the juncture edge of the cone to an arbitrary point on its surface is

$$x = y_0 - y \qquad [B.6]$$

where y_0 is the slant height of the cone. Further, if we define

$$\beta^4 = \frac{3\,(1-\nu^2)\cos^2\alpha}{h^2R_0^2} \qquad [B.7]$$

Equation [B.5] may then be rewritten in the form

$$\frac{d^4w}{dx^4} + 4\beta^4 w = 0 \qquad [B.8]$$

It should be noted that Equation [B.8] is identical in form to the homogeneous differential equation which governs the axisymmetric transverse bending displacements (and therefore the stresses) of a cylindrical shell as given on page 392 of Reference 2. For this reason the Geckeler approximation is sometimes referred to as the "equivalent cylinder" approximation. It is further noted that as the cone degenerates to a cylinder, i.e., $\alpha \to 0$, Equations [B.7] and [B.8] reduce exactly to those for a cylinder.

It should be emphasized that such so-called "approximate" methods are schemes to obtain simpler solutions to the exact Love-Meissner equations for the bending of shells. The membrane solutions for conical shells, which depend upon the loading and are particular integrals of the complete equation with a nonzero right-hand side, are very simple for the case of hydrostatic pressure loading; they should always be used with either the exact or the approximate bending solutions when the cone angle is not nearly equal to zero, i.e., $\alpha \geq 8$ deg. When the angle α is very nearly equal to zero, the radius R varies only slightly so that the membrane solution for a cylindrical shell is sufficiently accurate for superposition with a bending effect.

APPENDIX C

DERIVATION OF THE STRESS AND STRAIN EXPRESSIONS, EQUATIONS [1] THROUGH [5]

The stresses developed in the shell are given by

$$\sigma_x = \frac{N_x}{h} \pm \frac{6M_x}{h^2}$$
$$\sigma_\phi = \frac{N_\phi}{h} \pm \frac{6M_\phi}{h^2} \qquad [C.1]$$

where the upper sign is used for the outer fiber and the lower one for the inner fiber; this sign convention is retained throughout this appendix. The first expression of [C.1] is the total longitudinal or meridional stress given as the sum of the meridional compressive component* and the meridional bending component. The second expression is the total circumferential or hoop stress given as the sum of the hoop compressive component* and the hoop bending component.

The corresponding strains are determined from the two-dimensional Hooke's law to be

$$\epsilon_x = \frac{1}{E}(\sigma_x - \nu\sigma_\phi) = \frac{1}{Eh}\left(N_x - \nu N_\phi \pm \frac{6M_x}{h} \mp \nu\frac{6M_\phi}{h}\right)$$
$$\epsilon_\phi = \frac{1}{E}(\sigma_\phi - \nu\sigma_x) = \frac{1}{Eh}\left(N_\phi - \nu N_x \pm \frac{6M_\phi}{h} \mp \nu\frac{6M_x}{h}\right) \qquad [C.2]$$

The complete expressions for the stress couples and stress resultants pertaining to an axisymmetric conical shell are given in Reference 5. In terms of the sign convention of the present report these are

$$M_x = D\left(\frac{d^2w}{dx^2} - \frac{\nu \sin\alpha}{R}\frac{dw}{dx}\right)$$
$$M_\phi = D\left(\nu\frac{d^2w}{dx^2} - \frac{\sin\alpha}{R}\frac{dw}{dx}\right) \qquad [C.3]$$
$$Q_x = -D\left(\frac{d^3w}{dx^3} - \frac{\sin\alpha}{R}\frac{d^2w}{dx^2} - \frac{\sin^2\alpha}{R^2}\frac{dw}{dx}\right)$$

*Tensile if N_x, N_ϕ are positive.

$$N_\phi = -\frac{d}{dx}\left(\frac{R}{\sin\alpha} Q_x \tan\alpha\right) - \frac{pR}{\cos\alpha}$$

$$= D\tan\alpha\left(\frac{R}{\sin\alpha}\frac{d^4w}{dx^4} - 2\frac{d^3w}{dx^3} - \frac{\sin\alpha}{R}\frac{d^2w}{dx^2} - \frac{\sin^2\alpha}{R^2}\frac{dw}{dx}\right) - \frac{pR}{\cos\alpha}$$

[C.3]

$$N_x = Q_x \tan\alpha - \frac{pR}{2\cos\alpha}$$

where the flexural rigidity $D = \dfrac{Eh^3}{12(1-\nu^2)}$,

M_x is the moment in a meridional plane,

M_ϕ is the moment in a transverse plane,

Q_x is the transverse shearing force,

N_ϕ is the stress resultant in the ϕ-direction,

N_x is the stress resultant in the x-direction, and

p is the external hydrostatic pressure (replace p by $-p$ for internal pressure).

It should be noted that the terms containing p in Equations [C.3] are the membrane stress resultants obtained from membrane analysis for hydrostatic pressure loading.

From the same order-of-magnitude considerations as those used in Appendix B to derive Equation [C.8], it can be seen that the following approximate stress couples and stress resultants should be of sufficient accuracy:

$$M_x = D\frac{d^2w}{dx^2}$$

$$M_\phi = \nu M_x$$

$$N_x = Q_x \tan\alpha - \frac{pR}{2\cos\alpha}$$

[C.4]

$$N_\phi = D\frac{R}{\cos\alpha}\frac{d^4w}{dx^4} - \frac{pR}{\cos\alpha}$$

$$Q_x = -D\frac{d^3w}{dx^3}$$

It will now be shown that another term should be included in the expression for N_ϕ given by [C.4]. From Hooke's law [C.2] and the geometry of deformation it is seen that

$$\frac{1}{Eh}(N_\phi - \nu N_x) = \epsilon_\phi = -\frac{\bar{w}}{R}$$

so that

$$N_\phi = -\frac{Eh}{R}\bar{w} + \nu N_x \qquad [C.5]$$

By superposition,

$$\bar{w} = \bar{w}_{\text{bending}} + \bar{w}_{\text{membrane}}$$

i.e.,

$$\bar{w} = w_b \cos\alpha + \frac{pR^2}{Eh\cos\alpha}\left(1 - \frac{\nu}{2}\right) \qquad [C.6]$$

where w_b is that part of the transverse displacement w exclusive of the membrane component. If Equation [C.6] is evaluated at the shell edge $x = 0$, the edge coefficients, d, g, and f are obtained; see Equation [8]. The edge coefficients so derived differ only slightly from those given in Reference 6 which are believed to be exact.

If N_x from Equations [C.4] and $\bar{w}$ as given by [C.6] are substituted into [C.5], then

$$N_\phi = -\frac{Eh}{R} w_b \cos\alpha - \frac{pR}{\cos\alpha} + \nu Q_x \tan\alpha \qquad [C.7]$$

Further, if w_b is determined from Equation [B.8] and substituted into [C.7], then

$$N_\phi = D\frac{R}{\cos\alpha}\frac{d^4w}{dx^4} - \frac{pR}{\cos\alpha} + \nu Q_x \tan\alpha \qquad [C.8]$$

With the stress resultants N_x, N_ϕ, Q_x, and the stress couples M_x and M_ϕ thus determined, Equations [C.4] and [C.8], the expressions for the shell stresses σ_x and σ_ϕ, become:

$$\sigma_x = -\frac{pR}{2h\cos\alpha} - \frac{D}{h}\tan\alpha\frac{d^3w}{dx^3} \pm \frac{6D}{h^2}\frac{d^2w}{dx^2} \qquad [C.9]$$

$$\sigma_\phi = -\frac{pR}{h\cos\alpha} + \frac{D}{h}\frac{R}{\cos\alpha}\frac{d^4w}{dx^4} - \frac{\nu}{h}D\tan\alpha\frac{d^3w}{dx^3} \pm \frac{6\nu D}{h^2}\frac{d^2w}{dx^2} \qquad [C.10]$$

To express these stresses in terms of the edge and surface loadings and also the geometric and elastic properties of the shell, expressions for the deflection w and its various derivatives must be found. This is done by integrating the differential Equation [B.8]. The solution of this homogeneous differential equation is

$$w = e^{-\beta x}(c_1 \cos \beta x + c_2 \sin \beta x) + e^{\beta x}(c_3 \cos \beta x + c_4 \sin \beta x) \qquad [C.11]$$

where the constants of integration c_1, c_2, c_3, and c_4 are determined from the boundary conditions

$$\begin{aligned} &w \to 0 \text{ at } x \to \infty \\ &M_x = M_i \text{ at } x = 0 \\ &Q_x = Q_i \text{ at } x = 0 \end{aligned} \qquad [C.12]$$

where M_i and Q_i are the edge bending moment and shearing force, respectively. The first of these conditions requires that

$$c_3 = c_4 = 0 \qquad [C.13]$$

When the second and third conditions are satisfied,

$$c_1 = \frac{1}{2D\beta^3}(-Q_i + \beta M_i) \qquad [C.14]$$

$$c_2 = -\frac{M_i}{2D\beta^2} \qquad [C.15]$$

With these values for the constants, the solution for w becomes:

$$w = \frac{e^{-\beta x}}{2D\beta^3}\left[(-Q_i + \beta M_i)\cos \beta x - \beta M_i \sin \beta x\right] \qquad [C.16]$$

Successive derivatives of this deflection function are:

$$\begin{aligned} \frac{dw}{dx} &= -\frac{e^{-\beta x}}{D\beta^2}\left[-\frac{Q_i}{2}(\sin \beta x + \cos \beta x) + \beta M_i \cos \beta x\right] \\ \frac{d^2w}{dx^2} &= \frac{e^{-\beta x}}{D\beta}\left[-Q_i \sin \beta x + \beta M_i(\cos \beta x + \sin \beta x)\right] \\ \frac{d^3w}{dx^3} &= -\frac{e^{-\beta x}}{D}\left[Q_i(\cos \beta x - \sin \beta x) + 2\beta M_i \sin \beta x\right] \\ \frac{d^4w}{dx^4} &= \frac{\beta e^{-\beta x}}{D}\left[2Q_i \cos \beta x - 2\beta M_i(\cos \beta x - \sin \beta x)\right] \end{aligned} \qquad [C.17]$$

Substitution of Equations [C.17] into [C.9] and [C.10] gives for the stresses,

$$\sigma_x = -\frac{pR}{2h\cos\alpha} + \frac{2\beta}{h} M_i \tan\alpha \left[\frac{Q_i}{2\beta M_i} e^{-\beta x} (\cos \beta x - \sin \beta x) + e^{-\beta x} \sin \beta x\right]$$

$$\pm \frac{6M_i}{h^2} \left[e^{-\beta x} (\cos \beta x + \sin \beta x) - \frac{Q_i}{\beta M_i} e^{-\beta x} \sin \beta x\right] \qquad [C.18]$$

$$\sigma_\phi = -\frac{pR}{h\cos\alpha}\left(1 - \frac{\nu}{2}\right) - \frac{2R\beta^2}{h\cos\alpha} M_i \left[e^{-\beta x} (\cos \beta x - \sin \beta x) - \frac{Q_i}{\beta M_i} e^{-\beta x} \cos \beta x\right] + \nu \sigma_x$$

[C.19]

Therefore, Equations [C.18] and [C.19] for the stresses are identical with Equations [1] and [2], respectively, if the functions $\phi(\beta x)$, $\psi(\beta x)$, $\theta(\beta x)$ and $\zeta(\beta x)$ as defined by Equations [7] are substituted therein.

To derive Equations [3], [4], and [5] for the strain distributions it is merely necessary to substitute Equations [C.18] and [C.19] into the two-dimensional Hooke's law, Equation [C.2], which expresses the strains ϵ_x and ϵ_ϕ in terms of the stresses.

REFERENCES

1. Geckeler, J., "Über die Festigkeit achsensymmetrischer Schalen," Forschungsarbeiten auf dem Gebiete des Ingenieurwesens, Berlin, Germany, No. 276 (1926), pp. 1-52.

2. Timoshenko, S., "Theory of Plates and Shells," McGraw-Hill Book Company, Inc., New York (1940).

3. Dubois, F., "Über die Festigkeit der Kegelschale," Doctorate Dissertation, Zurich (1917).

4. Watts, G.W. and Burrows, W.R., "The Basic Elastic Theory of Vessel Heads under Internal Pressure," Journal of Applied Mechanics, Vol. 16 (1949), pp. 55-73.

5. Wenk, E., Jr., and Taylor, C.E., "Analysis of the Stresses at the Reinforced Intersection of Conical and Cylindrical Shells," David Taylor Model Basin Report 826 (Mar 1953).

6. Taylor, C.E. and Wenk, E., Jr., "Analysis of Stresses in the Conical Elements of Shell Structures," David Taylor Model Basin Report 981 (May 1956).

7. Borg, M.F., "An Investigation of the Stresses and Strains Near Intersections of Conical and Cylindrical Shells," David Taylor Model Basin Report 911 (Feb 1956).

8. Horvay, G., et al, "Analysis of Short Thin Axisymmetrial Shells Under Axisymmetrical Edge Loading," Journal of Applied Mechanics, Vol. 23 (Mar 1956), pp. 68-72.

INITIAL DISTRIBUTION

Copies	
14	CHBUSHIPS, Library (Code 312) 5 Tech Library 1 Tech Asst to Chief (Code 106) 2 Prelim Des (Code 420) 2 Hull Des (Code 440) 2 Sci and Res (Code 442) 2 Submarines (Code 525)
2	CHBUAER
2	CHONR, Mech Br (Code 438)
2	CDR, USNOL
1	DIR, USNRL
2	NAVSHIPYD NORVA, UERD (Code 270)
2	NAVSHIPYD PTSMH
2	NAVSHIPYD MARE
2	NAVSHIPYD NYK, USN Mat Lab
2	CDR, USNOTS, China Lake, Calif.
1	CO, USNUOS, Newport, R.I.
1	DIR, USNEES, Annapolis, Md.
2	DIR, USNAES, Nav Air Matl Ctr, Philadelphia, Pa Attn: Head, Aero Matl Lab
2	SUPT, USN Postgrad School, Monterey, Calif.
2	CO, USN Admin Unit, MIT, Cambridge, Mass.
1	CO, Redstone Arsenal, Huntsville, Ala.
2	ASTIA, Arlington, Va.
1	Army Ballistic Missile Agcy, Struc & Mech Lab, Huntsville, Ala.
3	SUPSHIPINSORD, Groton, Conn. 2 General Dynamics Corp, Electric Boat Div
3	SUPSHIPINSORD, Pascagoula, Miss. 2 Ingalls Shipbuilding Corp
3	SUPSHIPINSORD, Newport News, Va. 2 Newport News Shipbldg & Dry Dock Co.

Copies	
1	Pressure Vessel Res Com, New York, N.Y.
1	Dr. C.E. Taylor, Dept of Theo & Appl Mech, University of Illinois, Urbana, Ill.
1	Dr. E. Wenk, Jr., Dept of Engin Mech, Southwest Res Inst, San Antonio, Tex.
1	Mr. Cyril O. Rhys, Sr., Independent Consultant, Hampton Hall, Cranford, N.J.

NAVY DPPO PRNC WASH D C